Collaborative inverse modeling of nitrogen and phosphorus content in rice based on WOA-ELM

Fenghua Yu[1,2], Shuang Xiang[1], Zhonghui Guo[1], Honggang Zhang[1], Juchi Bai[1], Tongyu Xu[1,2*]

(1. *College of Information and Electrical Engineering, Shenyang Agricultural University, Shenyang 110866, China*;
2. *Liaoning Agricultural Information Engineering Technology Research Center, Shenyang 110866, China*)

Abstract: Nitrogen and phosphorus play an important role in the growth and development of crops, and the accurate acquisition of information on crop nitrogen and phosphorus nutrient levels is of great significance in terms of accurate crop management and saving planting costs.   To address the problem that previous single-element monitoring has led to difficulties in synergy between inversion models, this paper proposes a method based on a whale algorithm with an extreme learning machine to achieve synergistic inversion of nitrogen and phosphorus content in rice, and demonstrates the feasibility of using spectral data to invert nitrogen and phosphorus simultaneously.   In this paper, an unmanned aircraft hyperspectral remote sensing platform was used to acquire hyperspectral remote sensing images of the canopy of japonica rice at key fertility stages, and agronomic information was sampled simultaneously on ground.   The hyperspectral data were downscaled by principal component analysis (PCA) and discrete wavelet multiscale decomposition (DWT), and the filtered feature vectors were used as input and the measured nitrogen and phosphorus content as output.   Two models, the limit learning machine and the limit learning machine based on the whale algorithm, were used to collaboratively estimate the nitrogen and phosphorus content of japonica rice at critical fertility stages, and the following conclusions were drawn: 1) The inversion accuracy of both models for nitrogen The R^2 of the training set was above 0.64 and the R^2 of the validation set was above 0.56.   2) The dimensionality reduction method using wavelet decomposition was more representative than that of principal component analysis in filtering feature vectors, and it was the best for phosphorus inversion.   3) Overall, the WOA-ELM model was better than the ELM model in estimation, with the R^2 of nitrogen inversion reaching up to this model has greatly improved the efficiency of obtaining the nutrient content of rice leaves.

Keywords: rice, nitrogen, phosphorus, hyperspectral, whale algorithm, extreme learning machine

DOI: 10.33440/j.ijpaa.20220501.184

1   Introduction

In agricultural production, nitrogen and phosphorus are important nutrients for the growth and development of food crops. Accurate information on the nutrient levels of nitrogen and phosphorus is important for precise crop management, saving planting costs and controlling farmland surface pollution.   The abundance and deficiency of nitrogen and phosphorus in rice are similar in appearance, both resulting in fewer tillers, smaller, thinner leaves and yellowish colour of the plant[1], which are difficult to distinguish morphologically by the naked eye and are very likely to confuse the judgement of nitrogen and phosphorus deficiency, thus affecting the fertilization decision[2].

UAV hyperspectroscopy can rapidly and non-destructively capture the characteristics of the spectral changes of plants, thus reflecting the subtle changes of various substances in plants, thus achieving timely and rapid identification of nutrient stresses[2].   At present, scholars at home and abroad have done a lot of research on the use of UAV hyperspectral technology for rapid and accurate monitoring of crop nutrient information.   Among them, the research on nitrogen is relatively concentrated, and the spectral sensitive bands of nitrogen have been clarified[3], a number of spectral indices applicable to nitrogen diagnosis have been screened, and the spectral quantitative prediction equation of nitrogen content has been established[4].   Xu Tongyu[5] et al. constructed an inverse model of rice nitrogen content by optimizing the limit learning machine of the aspen whisker search algorithm based on the characteristic band spectra obtained from UVE screening.   Wang Jiaojiao[6] et al. found that the characteristic bands screened by using GPR were the best for nitrogen content model construction at the leaf and canopy scales of rice.   Yang Hongyun[7] et al. fed the spectral data processed by PCA and SPA into a support vector machine (SVM) to build a nitrogen content estimation model for rice, and the estimation accuracy reached 99.38%.   There are relatively few studies on phosphorus, and the results obtained are not uniform and need further validation.   Ban Songtao[8] et al. used partial least squares regression to establish a model for estimating phosphorus content in rice.   Quan Dongping[9] et al. used wavelet denoising, linear regression and

partial least squares to establish a model for monitoring phosphorus content in citrus, and achieved good results.Osborne et al.[10] showed that the blue light band (440-445 nm) and the near-infrared band (730-930 nm) could be used to monitor the severity of phosphorus deficiency in maize in the early stages, while the later stages or high soil phosphorus concentrations were not suitable for phosphorus content diagnosis.   Based on mutual information theory, Lin Fenfang et al[11] derived five spectrally sensitive bands for phosphorus content of rice leaves at the nodulation stage and used them to build a better network model, demonstrating the feasibility of using mutual information theory to invert the phosphorus content of rice.

Most previous crop nutrition tests have been established based on a single nutrient, but the identification and diagnosis of single nutrient deficiency symptoms cannot exclude changes in crop foliar characteristics caused by other nutrients, and the effects of multiple elements on rice growth and development are inextricably linked, with interactions between them[12].   Plant physiology also indicates that the uptake of nitrogen and phosphorus by rice is influenced by fertilization conditions, and there is an interaction and constraint between nitrogen and phosphorus[13-14].   In order to explore the influence of nitrogen and phosphorus interaction on rice canopy reflectance spectra and to avoid the problem of difficult synergy between inversion models for single element monitoring, this paper takes northeast japonica rice as the research object and uses an unmanned aircraft hyperspectral remote sensing platform to acquire hyperspectral remote sensing image information of the canopy of japonica rice at key fertility stages, with simultaneous ground sampling of agronomic information.   The inverse model of nitrogen and phosphorus content of japonica rice during the critical fertility period was established by using two methods, namely the limit learning machine and the limit learning machine based on the whale algorithm, to explore the feasibility of using spectral data to invert nitrogen and phosphorus simultaneously and its methods, with a view to providing a theoretical basis and method for the identification of nitrogen and phosphorus stress in field production, and at the same time providing scientific support for accurate rice The aim was to provide a theoretical basis and method for the identification of N and P stress in field production, and to provide scientific support for accurate fertilization decisions.

2   Materials and methods

2.1   Experimental design

The experiment was conducted from June to September 2021 at the precision agriculture aerial research base of Shenyang Agricultural University, Gengzhuang Town, Haicheng City, Anshan City, Liaoning Province (40°58'45.39"N, 122°43'47.0064"E), and the experimental data were collected under good weather conditions in order to obtain effective remote sensing images of the japonica rice canopy.   The experimental field was divided into two large areas, with five N fertilizer gradients in Experimental Area 1 with N0=0 kg/hm², N1=75 kg/hm², N2=150 kg/hm², N3=225 kg/hm², N4=300 kg/hm², and Experimental Area 2 with the same five N fertilizer gradients.   Again, five N fertilizer gradients were established, with N0=0 kg/hm², N1= 50 kg/hm², N2=100 kg/hm², N3=150 kg/hm², N4=200 kg/hm², and a N fertilizer basal chase ratio of 5:3:2, with three replications per gradient, for a total of 3×5 = 15 plots.   A total of 15 plots were established.   The area of each plot in Experiment 1 was 5×8= 40 m² and that of each plot in Experiment 2 was 660 m².   The

field management of the two experimental areas was the same except for the nitrogen fertiliser gradient.   The standard rate of potash application was 192 kg/hm², with a 1:1 ratio of base to chase, and the rest of the field management was the same as conventional high-yield management.   Phosphorus fertiliser was not treated as the application of N fertiliser also had an effect on the phosphorus content of the plants.   Sampling in the field was carried out from the tillering stage to the tasseling stage, with a sampling interval of 9 days.   In each experimental plot, a 1 m×1 m plot was randomly selected and framed with a plastic frame for subsequent identification of the area of interest, from which three representative holes of rice were selected for obtaining N and P concentrations.   A total of 325 sets of samples were collected for the experiment.

In order to avoid the impact of coarse errors generated during the experiment on the accuracy of the inversion, the outliers of the nitrogen and phosphorus content data measured in the experiment were removed by a 3-fold standard deviation method, while the abnormal spectral data were removed using the Monte Carlo algorithm to finally obtain a sample set of 312.
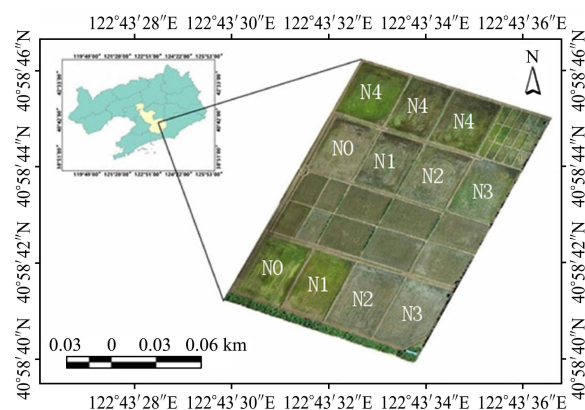
Figure 1   Map of experimental plots

2.2   Rice hyperspectral data acquisition

The UAV hyperspectral platform of the M600 PRO six-rotor UAV from DJI Innovation Shenzhen was used.   The hyperspectral imager was selected from the GaiaSky-mini built-in push-and-sweep airborne hyperspectral imaging system from Sichuan Shuangli Hopper, with a hyperspectral band range of 400~1000 nm, a resolution of 3nm and 253 effective bands.   The spatial resolution is 0.12 mm, the FOV is 31.34 °, the pixel spacing is 6.45 μm, and the lens diameter is 25 mm.   The UAV hyperspectral remote sensing platform data is collected daily from 11:00 a.m. to 12:00 p.m., when the sunlight intensity is stable and the UAV flight altitude is set at 150 m.   The collected image information needs to be extracted from the cell hyperspectral data by ENVI5.3+IDL software, and the interfering feature spectra are removed by the method of wave angle filling.   The average spectrum of each plot is calculated by filling in the spectral angle of the interfering features, and the average spectrum of each plot is resampled by matlab software to improve the spectral resolution to 1 nm, and the resampled spectral data is used as the hyperspectral information of each test plot.   The ENVI software was used to obtain the average rice spectral reflectance in the region of interest (ROI) of each plot, and used it as the rice canopy spectral reflectance of the plot.

2.3   Acquisition of agronomic parameters in rice

2.3.1 Determination of leaf nitrogen content

About 20 leaves from different parts of japonica rice were collected from each test plot, placed in self-sealing bags, marked with plot name and number, and brought back to the laboratory immediately.　In the room, the leaves were first washed to remove unwanted substances such as dust from the surface of the leaves, then the samples were dried at 80°C to a constant weight after being killed at 105°C for 30 min and weighed and crushed. Finally the plant nitrogen concentration was measured by Kjeldahl method, calculated as follows.

$$N_c = \frac{V \times 0.05 \times 0.014}{M} \times 100 \qquad (1)$$

where, N_c is the sample nitrogen concentration (%); V is the volume of hydrochloric acid solution (mL) and M is the sample mass.

The final statistical analysis of the 312 sets of effective nitrogen concentration data obtained resulted in the probability density histogram shown in Figure 2.
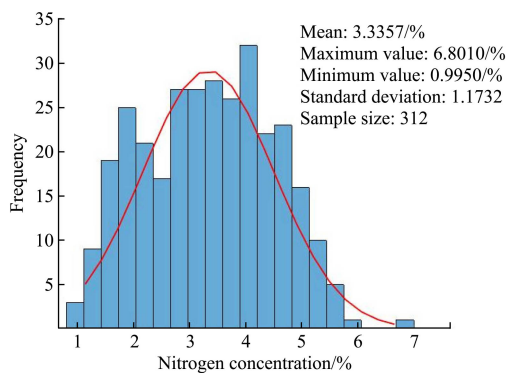
Figure 2　Probabilistic density function of nitrogen content in 312 groups of japonica rice leaves

As can be seen from Figure 2, the 312 sets of japonica rice leaf nitrogen concentration data were normally distributed with a mean value of 3.3357/%, a maximum value of 6.801/% and a minimum value of 0.995/% with a standard deviation of 1.1732, which is suitable for inversion of nitrogen content.　The Kennard-Stone algorithm (KS) was also used to divide the samples into a 7:3 ratio for the training and test sets, and the statistical table of nitrogen concentrations is shown in Table 1.

Table 1　Rice leaf nitrogen concentration statistics

(%)

Sample set	Sample size	Minimum set	Maximum set	Average	Standard deviation
Training set	218	0.995	5.863	3.4107	1.1312
Test set	94	1.145	6.801	3.1617	1.2544
Overall	312	0.995	6.801	3.3357	1.1732

2.3.2　Determination of leaf phosphorus content

To determine the phosphorus concentration of a sample, the previous procedure is the same as for the determination of the nitrogen concentration, except that the phosphorus concentration of the plant is measured by the vanadium-molybdenum yellow colourimetric method on the ground sample.　The calculation formula is as follows.

$$P \ (g/kg) = \frac{(C - C_0) \cdot V \cdot D}{m} \times 10^{-3} \qquad (2)$$

where, C - the mass concentration of the colour developing solution P, $\mu g/mL$; C_0 - Blank values, $\mu g/mL$; V - volume of colour developing liquid, mL; D - the fractionation multiple, i.e. the volume of disinfectant fixation (mL) / volume of disinfectant aspirated (mL); m - mass of dry sample, g.

The final statistical analysis of the 312 sets of effective nitrogen concentration data obtained resulted in the probability density histogram shown in Figure 2.

As can be seen from Figure 3, the phosphorus concentration data of 312 sets of japonica rice leaves were normally distributed with a mean value of 0.3242/%, a maximum value of 0.419/% and a minimum value of 0.214/%, with a standard deviation of 0.0446, meeting the requirements of nitrogen content inversion.　The Kennard-Stone algorithm (KS) was also used to divide the samples into a 7:3 ratio for the training and test sets, and the statistical table of phosphorus concentrations is shown in Table 2.
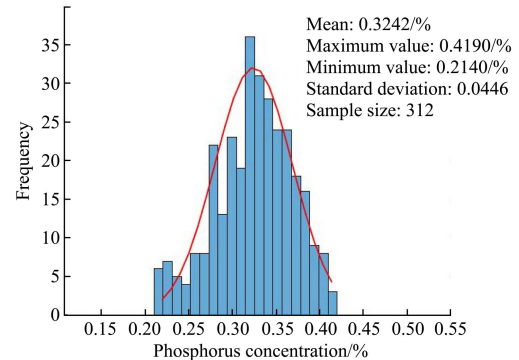
Figure 3　Probabilistic density function of phosphorus content in 312 groups of japonica rice leaves

Table 2　Rice leaf phosphorus concentration statistics

(%)

Sample set	Sample size	Minimum set	Maximum set	Average	Standard deviation
Training set	218	0.214	0.414	0.3231	0.0441
Test set	94	0.228	0.419	0.3268	0.0458
Overall	312	0.214	0.419	0.3242	0.0446

2.4　Hyperspectral feature band extraction

As full-band spectral data contains a large number of similar bands, the use of a large amount of redundant information for modelling often results in slower runs, higher model errors and lower inversion accuracy[15].　In order to reduce the number of input variables and to reduce the number of inversions, the model has to be used in the same way as the model.　In order to reduce the number of input variables, reduce data redundancy and improve the modelling speed and accuracy, this study decided to adopt two methods of feature extraction for hyperspectral data, namely Principal Component Analysis (PCA) and discrete wavelet multi-scale decomposition. as the main input of the model.

2.4.1　Principal component analysis

Principal component analysis (PCA) has been widely used in hyperspectral dimensionality reduction.　The basic idea of its dimensionality reduction is to project the spectral variables into the low-dimensional space by linear mapping, and the transformed spectral variables are ranked according to the variance contribution rate.　In order to ensure that the total variance information of the transformed spectral variables in the low-dimensional space is maintained as much as possible, i.e. to ensure the maximum independence between the generated new variables and the minimum loss of information, 98.918% of the principal components were selected as the input quantity of the model in this study.

2.4.2 Discrete wavelet multiscale decomposition

Wavelet analysis can achieve accurate decomposition of signals in the time and frequency domains, for different signals, the way in which they are decomposed varies, for the spectral information of leaves, its decomposition is equivalent to a series of transformations of spectral data in the spectral band, the expression of the wavelet basis function is

$$\phi_{a,b}(\lambda) = \frac{1}{\sqrt{a}}\phi\left(\frac{\lambda-b}{a}\right)a,b\in R;\ a>0;\ \int_{-\infty}^{+\infty}\phi(\lambda)d\lambda=0 \qquad (3)$$

where, a is the stretch factor; b is the translation factor; λ is the independent variable; and the mean value of the function is 0.

The discrete wavelet transform is a discretization of the translational and decomposition scales. $f(\lambda)$ as the input one-dimensional signal can be discretized by the discrete wavelet variation coefficient of equation (4) $W_{j,k}$ for the signal $f(\lambda)$ approximation.

$$W_{j,k} = (f(\lambda),\phi_{j,k}(\lambda)) \qquad (4)$$

where the wavelet basis function $\phi_{j,k}(\lambda)$ can be calculated by equation (5).

$$\phi_{j,k}(\lambda) = 2^{\frac{-j}{2}}\phi(2^{-j}\lambda - K) \qquad (5)$$

where, j,k are the jth layer decomposition and kth wavelet coefficients, respectively, and the discrete wavelet variant is usually chosen at the scale of a binary sequence, $j=2,4,8,..., 2^p, p\in N$, so that the calculation will be more efficient. When the signal is decomposed by the discrete wavelet transform multiscale, the resulting wavelet coefficients record the approximate coefficients of the low frequency signal and the detail coefficients of the high frequency signal. In general, the approximate coefficients of the wavelet signal better reflect the characteristics of the input variables, so the wavelet approximate coefficients are chosen as the input quantity for the inverse model[16].

2.5 Model construction and evaluation criteria

In this study, two methods, Extreme Learning Machine (ELM) and Whale Algorithm-based Extreme Learning Machine (WOA-ELM), were used for modelling, and the coefficients of determination of the prediction results of the training and test sets by the two models R^2. The inverse accuracy and robustness of the models were measured by the coefficient of determination and root mean square error (RMSE) of the prediction results of the two models on the training and test sets.

The Extreme Learning Machine (ELM) was originally proposed by Huang et al. of Nanyang Technological University[17]. The algorithm randomly generates the connection weights of the input and hidden layers during the initialisation process, and requires no adjustment during the training of the model, only the number of neurons in the hidden layer to be adjusted for optimisation. Compared with other traditional feedforward neural network training frameworks, it has significant advantages such as fast learning speed and simple implementation method[18]. However, its mechanism of randomly generating initial values tends to reduce the stability and generalisability of the model built[19]. Therefore, this study uses the whale algorithm to optimise the optimisation of the extreme learning machine.

The whale algorithm is divided into 3 main steps: encircling the prey, the spiral bubble net attack method, and randomly finding the prey.

(1) Surrounding the prey.

Since the target prey position is unknown a priori, the WOA algorithm considers the current position of the best candidate individual in the whale group as the target prey position, and the other individuals in the group update their position according to the position of the best candidate individual. That is.

$$D = |C \cdot X^*(t) - X(t)| \qquad (6)$$

$$X(t+1) = X^*(t) - A \cdot D \qquad (7)$$

where, X is a position vector representing the current orientation of the humpback whale; T is the number of iterations; A and C are both coefficient vectors; and X^* is the best solution for the currently obtained position of the whale population.

A and C are calculated as

$$A = 2ar - a \qquad (8)$$

$$C = 2r \qquad (9)$$

where, a decreases linearly from 2 to 0 according to the inverse of the number of iterations; r is a random vector from 0 to 1.

(2) Spiral bubble net attack method.

The WOA algorithm first calculates the distance between an individual whale and its target prey, and then simulates the hunting behaviour of a humpback whale in a spiral motion.

$$D' = |X^*(t) - X(t)| \qquad (10)$$

$$X(t+1) = D' \cdot e^{bl} \cdot \cos(2\pi l) + X^*(t) \qquad (11)$$

where, b is the constant factor defining the shape of the spiral and l is an arbitrary constant in the interval –1 to 1.

(3) Random hunting for prey

During predation, when A is greater than 1 or less than –1, individuals in the pod will randomly select prey with reference to each other's positions to improve the global search capability of the algorithm. Namely

$$D = |C \cdot X_{rand} - X| \qquad (12)$$

$$X(t+1) = X_{rand} - A \cdot D \qquad (13)$$

where, X_{rand} is the random position vector of the current whale population.

WOA optimises ELM in the following steps:

(1) Parameter initialization. Set the parameters of WOA: number of individual whales, maximum number of iterations, variable dimension, upper and lower variable limits.

(2) Population initialization. The location values of each dimension of all individual whales are randomly initialized, and the location values of each dimension of each individual whale represent the input weights or thresholds.

(3) Calculate the fitness value.

(4) Update the optimal solution. Find the location of the optimal solution among all solutions based on the fitness value of each individual whale, and update the location of each individual whale based on the location of the optimal solution.

(5) Position updates for each individual whale.

(6) Repeat steps (3)-(5) until the maximum number of iterations, obtain the best input weights and thresholds, and bring the best input weights and thresholds into the ELM network for further training.

In order to assess the accuracy and stability of the inverse model for nitrogen and phosphorus content of japonica rice leaves, this study used the coefficient of determination R^2 and root mean square error RMSE were used to test the fitting effect and estimation ability of the model. The equations are given in Eqs. (14) and (15).

$$R^2 = \frac{\sum_{i=1}^{n}(\hat{y}_l - \overline{y})^2}{(\hat{y}_l - \overline{y})^2} \qquad (14)$$

$$RMSE = \sqrt{\frac{\sum_{i=1}^{n}(\hat{y}_l - y_i)^2}{n}} \qquad (15)$$

3   Results and analysis

3.1   Screening of spectral feature band

3.1.1   PCA selection of effective feature bands

Given that the full-band spectral data contains a large number of similar bands, it has a greater impact on the efficiency and accuracy of modelling.   Therefore, firstly, principal component analysis was used to initially select the characteristic bands to form a set of unrelated composite variables to replace the original spectral data, which greatly reduced the redundant information in the spectral data.   The group of unrelated variables was ranked from the largest to the smallest, and finally the top five principal components with a cumulative contribution of over 98.918% were selected as input variables for modelling.

3.1.2   Selection of spectral features by discrete wavelet multiscale decomposition

The determination of the wavelet mother function and the best decomposition scale is one of the key aspects of wavelet decomposition for feature extraction.   If the discrete wavelet transform of the spectral signal is multi-scale, the wavelet mother function and the decomposition scale can be considered as the best choice if the decomposed wavelet information can reflect both the profile characteristics of the spectrum and the purpose of compressing the data[20].

First, using the db10, coif5, sym8 wavelet mother functions for a sample data 2^j (j=1,2,...,12) scales, denoted as Level 1 to 12 (Level 1 to 12).   The number of levels of spectral decomposition is set to 12, and an input spectral signal is decomposed to produce a vector of approximate coefficients (on level 12) and 8 vectors of details (on level 1~12).   Figure 4a shows how the ratio of the number of decompositions varies with the number of decomposition layers.   It can be seen that as the number of decomposition layers increases, the number of wavelet coefficients generated per layer decreases, with the sym8 wavelet mother function being the most effective for the decomposition of spectral signals.   This multi-frequency decomposition better reflects the low-frequency information of the signal.   Therefore, the approximate coefficients of each layer under the db10, coif5 and sym8 wavelet mother functions were reconstructed, and the correlation coefficients of each reconstructed spectral signal and the original spectral signal were calculated, as shown in Figure 4b and Table 3.
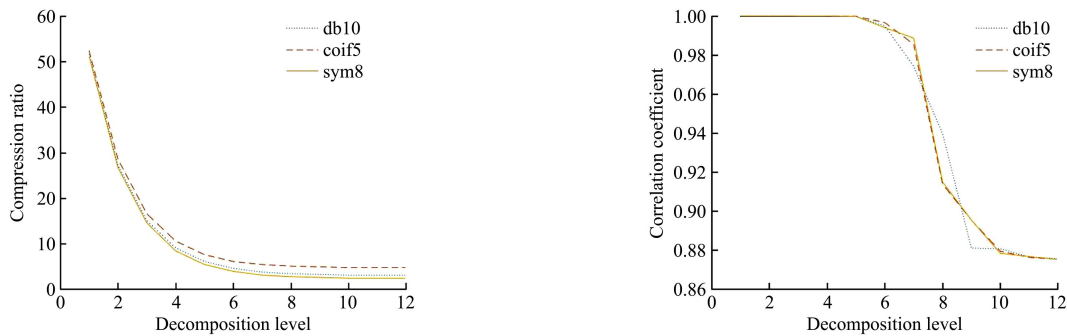
a. Changes of compression ratio with number of decomposition layers   b. Changes of correlation coefficient with the number of decomposition layers

Figure 4   Compression rate and correlation coefficient under different wavelet generating functions

Table 3   Number of decomposition level under different wavelet generating functions

Decomposition level	db10			coiff5			Sym8		
	Correlation coefficient	Approximate number	Compression ration	Correlation coefficient	Approximate number	Compression ration	Correlation coefficient	Approximate number	Compression ration
1	1	310	51.495	1	315	52.326	1	308	53.163
2	1	164	27.243	1	172	28.571	1	161	26.744
3	1	91	15.116	1	100	16.611	1	88	14.618
4	1	55	9.136	1	64	10.631	1	51	8.472
5	1	37	6.146	1	46	7.641	1	33	5.482
6	0.995	28	4.651	0.997	37	6.146	0.994	24	3.967
7	0.975	23	3.821	0.986	33	5.481	0.969	19	3.156
8	0.940	21	3.489	0.914	31	5.150	0.915	17	2.824
9	0.881	20	3.222	0.895	30	4.983	0.895	16	2.658
10	0.880	19	3.156	0.879	29	4.817	0.878	15	2.492
11	0.876	19	3.156	0.876	29	4.817	0.877	15	2.492
12	0.875	19	3.156	0.875	29	4.817	0.875	15	2.492

From Table 3, we can see that among the three wavelet mother functions, the coif5 wavelet mother function has the largest number of approximate coefficients, the highest compression ratio, and the data compression effect is not very good, the sym8 wavelet mother function has the smallest number of approximate coefficients, the highest compression ratio, and the best data compression ability, and the de10 wavelet mother function has the general data compression effect. When the number of decomposition layers reaches 7, the number of approximation coefficients of the three wavelet mother functions tends to stabilize, among which, the

number of approximation coefficients of sym8 wavelet mother function is the lowest. Considering the compression effect and the number of approximation coefficients of various wavelet mother functions, the sym8 wavelet mother function is chosen and the best effect is used for decomposition when the number of decomposition layers is 7.

The essence of the different scales in the discrete wavelet transform is to filter the signal with band-pass filters of various centre frequencies. The low-frequency approximate wavelet coefficients reflect the significant absorption characteristics of the original spectrum and represent the overall shape of the spectrum, and by combining the decomposed low-frequency approximate wavelet coefficients for the inverse transform, the accuracy of the inversion will be improved.

3.2 Inverse modelling and analysis of nitrogen and phosphorus content of japonica rice leaves

3.2.1 Extreme learning machine inversion modelling

The inverse model of nitrogen and phosphorus content of rice leaves based on extreme learning machine (ELM) was constructed by taking the results of dimensionality reduction by PCA and DWT as the input of the model and the measured nitrogen and phosphorus content of rice leaves as the output, and setting the parameters of ELM as follows: the activation function is Sin, and the number of neurons in the hidden layer of the feature vector using PCA The number of neurons in the hidden layer was adjusted to 45 for the feature vector using PCA and 60 for the feature vector using discrete wavelet decomposition, which resulted in the best inversion. R^2 the modelling results are shown in Figure 5.
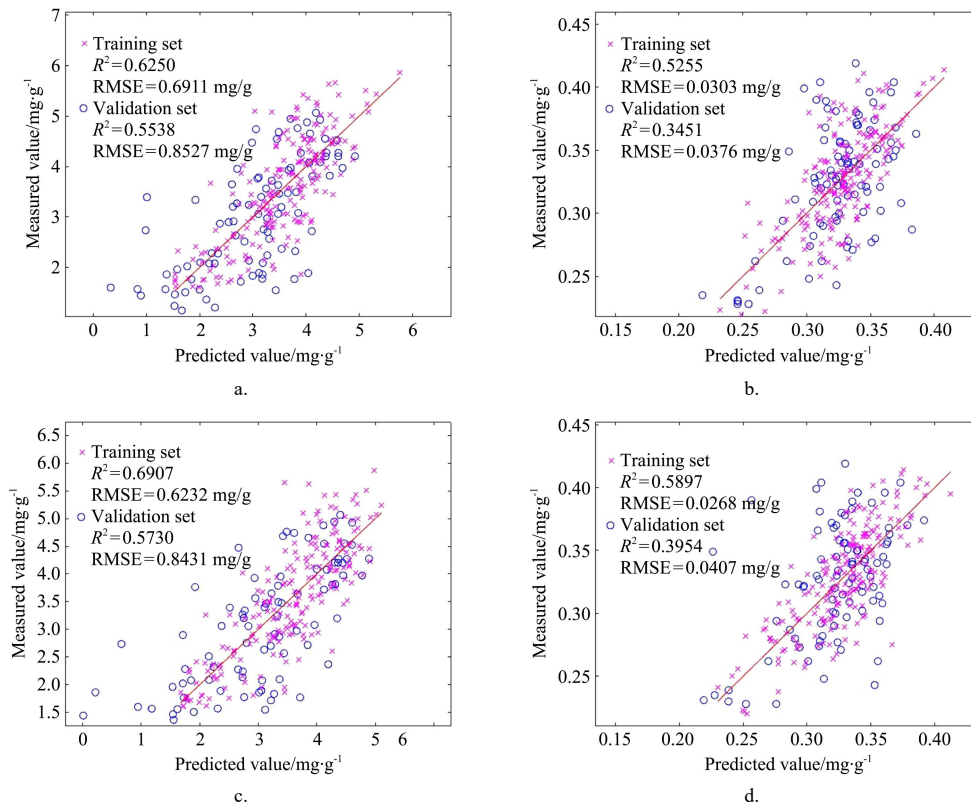
Note: a-b are the results of nitrogen and phosphorus inversions of the original hyperspectrum after extracting the eigenvectors by PCA, c-d are the results of nitrogen and phosphorus inversions of the original hyperspectrum after extracting the eigenvectors by discrete wavelet decomposition, respectively.

Figure 5   Extreme Learning Machine inversion results

The results analysis table is shown in Table 4. From the table, it can be seen that the inversion effect of both methods for nitrogen and phosphorus is average, among which, the inversion effect for nitrogen is better than that for phosphorus, and the correlation coefficients of both the training set and the test set reach above 0.55. The comparison of the two feature extraction methods concludes that the feature vectors screened from hyperspectral data using the discrete wavelet multi-scale decomposition method for the inversion of rice nitrogen and phosphorus content better.

Table 4

Element	Methods	Training set		Test set	
		Decision factor	RMSE	Decision factor	RMSE
Nitrogen	Principal component analysis	0.625	0.6911	0.5538	0.8527
	Multiscale decomposition of discrete wavelets	0.6907	0.6232	0.573	0.8431
Phosgene	Principal component analysis	0.5255	0.0303	0.3451	0.0376
	Multiscale decomposition of discrete wavelets	0.5897	0.0268	0.3954	0.0407

3.2.2 Extreme learning machine inversion modelling based on the whale algorithm

The feature vectors obtained by PCA and DWT were used as the independent variables of the model and the nitrogen or phosphorus content as the dependent variables, respectively, and input into the whale optimization algorithm-extreme learning machine (WOA-ELM) for training and testing, in this model, the population In this model, the number of populations was set to 50 and the number of iterations was set to 50. The convergence effect of WOA is shown in Figure 6, from which it can be seen that the value of the fitness function is basically constant when the

number of iterations is close to 50. The model accuracy was evaluated using the coefficient of determination R^2 and root mean square error RMSE, and the model inversion results are shown in Figure 7.
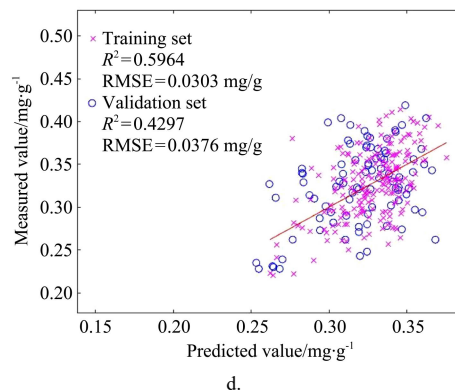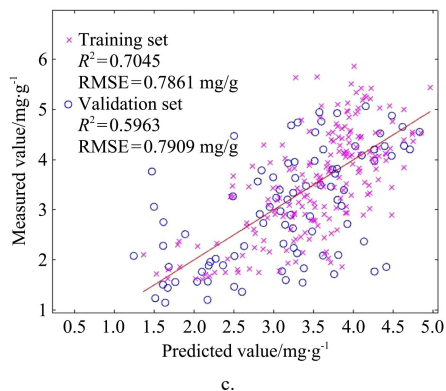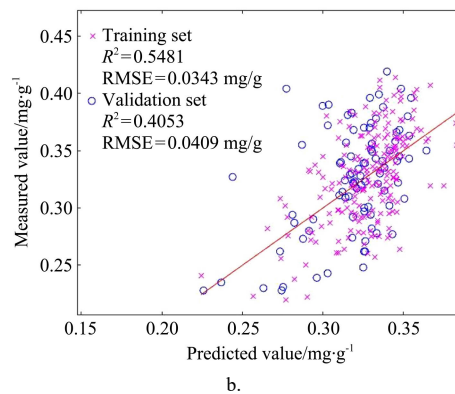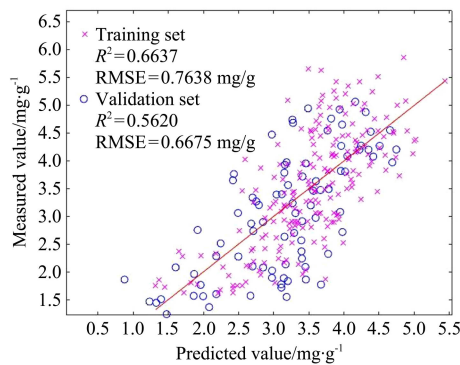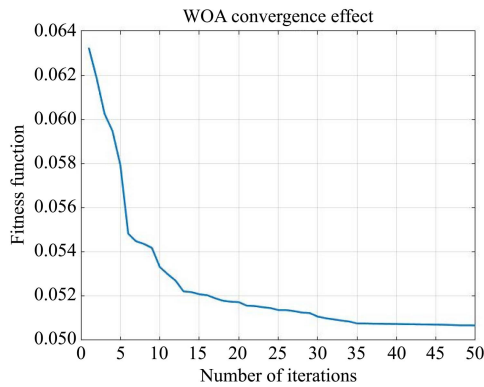
Figure 6　WOA convergence effect

The results analysis table is shown in Table 5, from which it can be seen that both feature extraction methods are more effective for rice nitrogen and phosphorus inversion, where. The feature vectors extracted by the method of discrete wavelet multi-scale decomposition were better for the inversion, with the nitrogen training set R^2 was 0.7045, the RMSE was 0.7862, the phosphorus R^2 was 0.5964 with an RMSE of 0.0344. Overall, the accuracy of the nitrogen inversion was greater than that of the phosphorus inversion, which was consistent with the results of the inversion using the extreme learning machine.

Note: a-b are the results of nitrogen and phosphorus inversions of the original hyperspectrum after extracting the eigenvectors by PCA, c-d are the results of nitrogen and phosphorus inversions of the original hyperspectrum after extracting the eigenvectors by discrete wavelet decomposition, respectively.

Figure 7　Plot of WOA-ELM inversion results

Table 5　Comparison of the coefficient of determination and RMSE for the inversion results of the extreme learning machine based on the whale algorithm

Element	Methods	Training set		Test set	
		Decision factor	RMSE	Decision factor	RMSE
Nitrogen	Principal component analysis	0.6637	0.7636	0.5620	0.6675
	Multiscale decomposition of discrete wavelets	0.7045	0.7861	0.5963	0.7909
Phosgene	Principal component analysis	0.5481	0.0343	0.4053	0.0409
	Multiscale decomposition of discrete wavelets	0.5964	0.0344	0.4297	0.0431

4　Discussion

As nitrogen and phosphorus are essential nutrients for crop growth, accurate information on nitrogen and phosphorus nutrient levels is important for precise crop management, saving planting costs and controlling farmland surface pollution. Previous studies have mostly focused on the effects of single levels of nitrogen and phosphorus on crop spectra, while capturing both nitrogen and phosphorus nutrient indicators in complex spectral information can provide a faster grasp of the full range of growth information and nutrient levels in rice.

In this study, the UAV imaging hyperspectral remote sensing platform was used to acquire hyperspectral remote sensing images of japonica rice, and the agronomic information was collected simultaneously on the ground. In terms of hyperspectral feature extraction, a cumulative contribution of 98.918% principal components obtained by principal component analysis was used as

the main input to the model, and a total of five principal components were obtained. This is due to the small sample size and the fact that the contribution of each component to the principal component in the principal component analysis is measured by the magnitude of the variance, which tends to be stable when the sample size is larger and a small amount of data is contingent and may have an impact on the results of the principal component analysis. The variance tends to stabilise when the sample size is larger, and a small amount of data is contingent and may affect the results of the principal component analysis. The results of dimensionality reduction from the method of discrete wavelet multi-scale decomposition are shown in Figure 4b, which shows the change of correlation coefficient between the reconstructed spectral signal and the original spectral signal for different decomposition layers. It can be seen that the correlation coefficient decreases rapidly as the number of decomposition layers increases and tends to stabilise when the number of decomposition layers reaches 12. According to previous studies, the model is very sensitive to the number of decomposition layers where the wavelet coefficients are located when constructing the inversion model, so the choice of scale is important. If the scale is too small, the noise cannot be effectively removed and the prediction accuracy cannot be improved. In this study, a 12-layer decomposition was chosen. In this study, the number of decomposition layers of 12 can not only improve the prediction accuracy of the model, but also improve the robustness of the model and make the prediction results more stable.

The feature vectors obtained after principal-form analysis and discrete wavelet multiscale decomposition and dimensionality reduction were used as input quantities respectively, and the nitrogen and phosphorus contents of rice measured by chemical experiments were used as output quantities to construct a simultaneous inversion model of rice nitrogen and phosphorus contents based on limit learning machine and whale algorithm. From the effect of inversion, the two inversion models were better than phosphorus for rice nitrogen content, which was due to the relatively low phosphorus content and the uneven distribution of data in the range, which caused more difficulty for inversion, which was consistent with the results of previous studies. Among them, ELM's inversion model had better inversion results for both nitrogen and phosphorus in the training set, but the difference between the validation set and the training set was larger, and the phenomenon of overfitting occurred, with weak generalization ability, which failed to achieve accurate inversion of rice nitrogen and phosphorus contents well. This is due to the fact that ELM randomly generates the connection weights between the input and hidden layers and the threshold values of the neurons in the hidden layer, and there is no need to adjust them during the training process, only the number of neurons in the hidden layer needs to be set in order to find the optimal solution. This method tends to fall into local minima, resulting in poor stability of the results. In comparison, the WOA-ELM inversion model has better inversion results, and the difference between the validation and training sets has decreased. Therefore, the WOA-ELM inversion model has slightly better inversion results, the difference between the validation and training sets has decreased, and the test results are more accurate, with the strongest generalisation ability and the highest recognition accuracy. This is due to the fact that the WOA-ELM model uses the WOA algorithm to optimize the optimization mechanism of ELM, which overcomes the disadvantages of random initialization of parameters in the input and implicit layers of ELM, and improves the global search ability of the network, so that the network has better recognition accuracy.

This paper proposes a monitoring method for simultaneous inversion of rice nitrogen and phosphorus content based on the extreme learning machine of the whale algorithm, and although the model inversion is good, there are still several shortcomings. In real rice fields, there are many factors that affect the hyperspectral data, so the nitrogen and phosphorus inversion model proposed in this study has significant limitations. Therefore, in future studies, stable nutrient prediction models need to be developed by expanding the data of rice varieties, different years and different paddy environments.

5   Conclusion

This paper is based on rice plot trials with different N fertilizer application treatments, destructive sampling method to obtain rice leaves at full fertility, using chemical experimental methods to obtain leaf nitrogen and phosphorus content, using principal component analysis and discrete wavelet multi-scale decomposition method to extract hyperspectral characteristic wavelengths, using the two methods to construct rice leaf N and P elemental content inversion models and compare their differences, the main conclusions are as follows.

(1) For hyperspectral data, two methods, principal component analysis and discrete wavelet multiscale decomposition, were used to filter feature vectors for simultaneous inversion of phosphorus and nitrogen, and the feature vectors extracted using the discrete wavelet multiscale decomposition method achieved the best modelling results in model prediction, and the study determined the optimal number of wavelet decomposition layers to be 12 and the wavelet mother function to be 'sym8'.

2) Overall, the inversion of the model is better for nitrogen than for phosphorus, due to the relatively low phosphorus content and the uneven distribution of the data over the range, which makes the inversion more difficult, and further improvements in the accuracy of the model are needed in future studies.

(3) ELM and WOA-ELM were used to construct the inverse models of nitrogen and phosphorus contents of rice leaves, respectively. The results showed that the estimation effect of the WOA-ELM model was better than that of the ELM model, with nitrogen inversions R^2 up to 0.7045 and the phosphorus inversion R^2 up to 0.4297.

The inverse model of nitrogen and phosphorus content of rice leaves can simultaneously estimate two nutrients in rice leaves, which greatly improves the efficiency of obtaining the nutrient content of rice leaves and ensures the accuracy of the estimation results and the stability of the model, providing a new method for accurately obtaining the elemental content of nitrogen and phosphorus in rice[34-35].

[References]

[1]   Thomas J R , Oerther G F . Estimating Nitrogen Content Of Sweet Pepper Leaves by Reflectance Measurements. Agronomy journal, 1972, 64(1): 11–13. Doi: 10.2134/agronj1972.00021962006400010004x.

[2]   Kokaly R F. Investigating a Physical Basis for Spectroscopic Estimates of Leaf Nitrogen Concentration. Remote Sensing of Environment, 2001, 75(2): 153–161. Doi: 10.1016/S0034-4257(00)00163-2.

[3] Osborne S L, Schepers J S, Francis D D , et al. Detection of Phosphorus and Nitrogen Deficiencies in Corn Using Spectral Radiance Measurements. Agronomy Journal, 2002, 94(6). Doi: 10.2134/agronj2002.1215.

[4] Huang G B , Zhu Q Y , Siew C K. Extreme learning machine: Theory and applications. Neurocomputing, 2006, 70(1/3): 489–501. Doi: 10.1016/ j.neucom.2005.12.126.

[5] Gupta R K, Vijayan D, Prasad T S. Comparative analysis of red-edge hyperspectral indices. Advances in Space Research, 2003, 32(11): 2217–2222. Doi: 10.1016/S0273-1177(03)90545-X.

[6] Haboudane D. Hyperspectral vegetation indices and novel algorithms for predicting green LAI of crop canopies: Modeling and validation in the context of precision agriculture. Remote Sensing of Environment, 2004, 90. Doi: 10.1016/j.rse.2003.12.013.

[7] Broge N H, Leblanc E. Comparing prediction power and stability of broadband and hyperspectral vegetation indices for estimation of green leaf area index and canopy chlorophyll density. Remote Sensing of Environment, 2001, 76(2): 156–172. Doi: 10.1016/ S0034-4257(00)00197-8.

[8] Chen P, Haboudane D, Tremblay N, et al. New spectral indicator assessing the efficiency of crop nitrogen treatment in corn and wheat. Remote Sensing of Environment, 2010, 114(9): 1987–1997. Doi: 10.1016/j.rse.2010.04.006.

[9] Li B, Liew O W, Asundi A K. Pre-visual detection of iron and phosphorus deficiency by transformed reflectance spectra. Journal of Photochemistry & Photobiology B Biology, 2006, 85(2): 131–139. Doi: 10.1016/ j.jphotobiol.2006.06.005.

[10] K Müller, Bttcher U, Meyer-Schatz F, et al. Analysis of vegetation indices derived from hyperspectral reflection measurements for estimating crop canopy parameters of oilseed rape (*Brassica napus* L.). Academic Press, 2008(2). Doi: 10.1016/J.BIOSYSTEMSENG.2008.07.004.

[11] Fitzgerald G, Rodriguez D, Garry O. Measuring and predicting canopy nitrogen nutrition in wheat using a spectral index：The canopy chlorophyll content index (CCCI). Field Crops Research, 2010, 3(116): 318–324.

[12] Burgos, X.P., Angela, R., Alberto, T., Gonzalo, P. Analysis of natural images processing for the extraction of agricultural elements. Image and Vision Computing, 2010, 28(1): 138–149. Doi: 10.1016/ j.imavis.2009.05.009.

[13] Xu G L, Zhang F L, Shah, et al. Use of leaf color images to identify nitrogen and potassium deficient tomatoes. Pattern Recognition Letters, 2011, 32(11): 1584–1590. Doi: 10.1016/ j.patrec.2011.04.020.

[14] Cai W S, Li Y K, Shao X G．A variable selection method based on uninformative variable elimination for multivariate calibration of near-infrared spectra．Chemometrics and Intelligent Laboratory Systems, 2008, 90(2): 188–194. Doi: 10.1016/j.chemolab.2007.10.001.

[15] Osborne S L, Schepers J S, Francis D D, Schlemmer M R. Detection of phosphorus and nitrogen deficiencies in corn using spectral radiance measurements. Agronomy Journal, 2002, 94: 1215–1221. Doi: 10.2134/agronj2002.1215.

[16] Menesatti P, Antonucci F, Pallottino F, Roccuzzo G, Allegra M, Stagno F, Intriglioio F. Estimation of plant nutritional status by Vis-NIR spectrophotometric analysis on orange leaves. Biosystems engineering, 2010, 105(4): 448–454. Doi: 10.1016/ j.biosystemseng.2010.01.003.

[17] Bronson K F, Chua T T, Booker J D, et al.. In-season nitrogen status in irrigated cotton II leaf nitrogen and biomass. Soil Science Society of American Journal, 2003(07): 1439–1448.

[18] Hamm J, Lee D. Separating pose and expression in face images: a manifold learning approach. Neural Information Processing-Letters and Reviews, 2007(04): 91–100.

[19] Ma J F, Yamaji N, Mitani N, et al. Transporters of arsenitein rice and their role in arsenic accumulation in rice grain. Proceedings of the National Academy of Sciences ofthe United States of America, 2008, 105(29): 9931–9935. Doi: 10.1073/pnas.0802361105.

[20] Asmhm Talukder, Ca Meisner, Mar Sarkar, et al. Effect ofwater management, arsenic and phosphorus levels on ricein a high -arsenic soil -water system: II. arsenic uptake .Ecotoxicology Environmental Safety, 2012, 80(80): 145–151. Doi: 10.1016/S1672-6308(13)60172-9 .